Dielectric Dispersion and AC Conductivity of Acrylonitrile Butadiene Rubber-Poly(vinyl chloride)/Graphite Composite

S. A. Mansour,[1,2] M. E. Al-ghoury,[3] E. Shalaan,[2] M. H. I. El Eraki,[2] E. M. Abdel-Bary[4]

[1]*Rabigh Faculty of Science and Arts, Department of Physics, King Abdul Aziz University, Saudi Arabia*
[2]*Faculty of Science, Department of Physics, Suez Canal University, Ismailia, Egypt*
[3]*Faculty of Science, Department of Physics, Sana'a University, Sana'a, Yemen*
[4]*Department of Chemistry, Faculty of Science, Mansoura University, Egypt*

Received 27 May 2009; accepted 28 January 2011
DOI 10.1002/app.34240
Published online 21 May 2011 in Wiley Online Library (wileyonlinelibrary.com).

ABSTRACT: Dielectric properties and ac electrical conductivity of Acrylonitrile Butadiene Rubber-poly(vinyl chloride)/Graphite Composite were studied at different frequencies (10^2–10^6 Hz) in the temperature range (298–423 K). The results show that the dielectric constant (ε'), dielectric loss (ε''), ac electrical conductivity (σ_{ac}) and, the electric modulus are strongly dependent on the frequency and temperature. The dielectric constant ε' increases with temperature and decreases with frequency, whereas the dielectric loss ε'' displays a broad maximum peak whose position shifts with temperature to a higher frequency region. Cole–Cole diagrams have been used to investigate the frequency dependence of the complex impedance at different temperature and graphite loading. Interfacial or Maxwell-Wagner-Sillars relaxation process was revealed in the frequency range and temperature interval of the measurements, which was found to follow the Havriliak–Negami approach for the distribution of relaxation times. At constant temperature, the frequency dependence of ac conductivity was found to fit with the established equation $\sigma_{ac}(\omega) = A\omega^s$ quite well. The values of S for the investigated samples lie between 0.88 and 0.11. The conduction mechanism of ac conduction was discussed by comparing the behavior of the frequency exponent S(T) with different theoretical models. It was found that the correlated barrier hopping (C.B.H.) is the dominant conduction mechanism. © 2011 Wiley Periodicals, Inc. J Appl Polym Sci 122: 1226–1235, 2011

Key words: dielectric properties; composites; poly(vinyl chloride); charge transport

INTRODUCTION

In recent years, several polymer blends have been commercially exploited. Their importance arises from the new and desirable properties absent in the homopolymers. The production of such polymer blends makes it possible to improve the physical properties of the individual polymers and, consequently, offers an economical way of designing new polymeric materials with improved properties. Polymeric blends are well established in the field of high-temperature insulation due to their low cost, ease of availability, and their outstanding electrical, chemical, and high-temperature resistance properties. A conducting polymer composite can be formed by dispersing conducting filler in sufficient quantity in a polymeric resin. Graphite powder[1–4] and carbon black,[5–8] have been used extensively as conducting filler. The electrical conductivity of conducting polymer composites can be increased with the addition of conducting filler. The composites undergo an insulator-conductor transition at a certain filler concentration, which is known as the percolation threshold (Pc). Insulator–conductor transition behavior of the composites near the Pc is explained by percolation theory.[9,10] Besides electrical conductivity, the presence of conducting additive particles affects substantially the dielectric behavior of the final composite. Maxwell–Wagner interfacial polarization resulted in moderate increases in ε' and ε'' below Pc. The dielectric constant of conducting polymer composites also increases with the addition of conducting filler. Especially, near the percolation threshold, a sharp change in the dielectric constant is observed. At the percolation threshold, many conducting particles are isolated by thin insulating layers. Therefore, near the percolation threshold, the composites can become a capacitor and consequently, can be applied in charge storing devices, and decoupling capacitor applications. Dramatic increase of dielectric constant close to the percolation threshold observed in the insulator–conductor percolative system arouse interest of developing conductive metal/polymer composites for embedded capacitor applications. Various metal fillers, such as silver, aluminum, and nickel have

Correspondence to: S. A. Mansour (saidhsa@yahoo.com.).

TABLE I
Formulation of (NBR-PVC)/Graphite Composite

Sample ingredients (phr)[a]	G_0	G_{10}	G_{20}	G_{30}	G_{40}	G_{50}	G_{60}	G_{70}
NBR	30	30	30	30	30	30	30	30
PVC	70	70	70	70	70	70	70	70
Graphite	0	10	20	30	40	50	60	70
Stearic acid	2	2	2	2	2	2	2	2
Zinc oxide	5	5	5	5	5	5	5	5
DOP[b]	35	35	35	35	35	35	35	35
MBTS[c]	1.5	1.5	1.5	1.5	1.5	1.5	1.5	1.5
TMTD	0.5	0.5	0.5	0.5	0.5	0.5	0.5	0.5
PBN[d]	1	1	1	1	1	1	1	1
Sulfur	2	2	2	2	2	2	2	2

[a]means all ingredients in (phr) relative to NBR.
[b]Dioctyle phthalate.
[c]MBTS is dibenzthiazyl disulphide.
[d]PBN is phenyl-β-naphthyl-amine, a possible carcinogenic compound.

been used to prepare the metal/polymer composite.[11–16] This material option represents advantageous characteristics over the conventional ceramic/polymer composites, especially ultra-high dielectric constant with balanced mechanical properties including the adhesion strength. Polymer/graphite composites are promising materials for embedded capacitors. They combine the high dielectric constant of graphite powders and the process capability and flexibility of polymers. The electrical conduction properties of polymer-graphite composites have been reported,[1–8] whereas the dielectric behavior has not been extensively reviewed.[17] In our recent work,[18,19] we examined the basic characteristics of the thermophysical properties (thermal conductivity, thermal diffusivity, and heat capacity) of nitrile rubber (NBR)/poly(vinyl chloride) (PVC) blends were measured in the temperature range of 300–425 K.[18] In the same work, the Agari–Uno model best predicted the effective thermal conductivity for the whole range of blend ratios and for the whole range of graphite contents in NBR/PVC (30/70)/graphite composites.[19] Have reported on the electrical properties and transport conduction mechanism of NBR/PVC Blend. The present work is a continuation of a program to study the dielectric properties of (NBR/PVC)/Graphite Composite in the aim of finding some suitable applications. Dielectric constant, dielectric loss, impedance, and ac conductivity have been determined and analyzed at different temperatures and frequencies.

MATERIALS AND METHODS

Composites preparation and properties

NBR [density 0.98 g/cm^3; acrylonitrile content = 34%; Mooney viscosity ML (1 + 4) at 100°C = 45 + 5 (ASTM D 1646); Average molecular weight = 163,376; glass temperature = −36°C], suspension polymerized PVC in a powder form [density = 1.38 g/cm^3; *K* value (molecular mass) = 66–69; melting point = 80°C; glass temperature = 87°C], and the other compounding ingredients listed in Table I and used for preparing the blends were supplied by Transport and Engineering (Alexandria, Egypt). Graphite powder from Merck (Germany) with a bulk density of 20–30 g/100 mL and a particle size of less than 50 mL was used too. The formulations of the blends are shown in Table I. The blends were prepared on a conventional laboratory-size rubber mill with a diameter of 150 mm, a working distance of 300 mm, a slow roll speed of 18 rpm, and a gear ratio of 1.4. The mixing occurred for 40 min at 298 K, and it was left for 24 h before vulcanization. Crosslinked samples of the desired thickness were produced by compression molding at 425 K and about 0.4 MPa for 30 min in an electrically heated press (Karl Kolb, Germany).

Measurements

Dielectric measurements

Dielectric relaxation spectra of the samples (discs of 10 mm diameter were cut from the molded plates) were obtained by a Hioki 3531z Hitester, Hioki, Japan, LCR, which is fully computerized with guard electrodes in the frequency range of 10^2–10^6 Hz. AC conductivity (σ_{ac}) has been evaluated from dielectric data in accordance with the relation:

$$\sigma_{ac} = \omega\varepsilon_0\varepsilon' \tan\delta \quad (1)$$

where ω is $2\pi rf$ (*f* is frequency), ε_0 is permittivity of the vacuum and dielectric constant (relative permittivity) ε' where C_p is the observed capacitance of the sample and C_o is vacuum capacitance of the cell and is calculated using the expression $\varepsilon_0 A/d$ (*A* and *d*

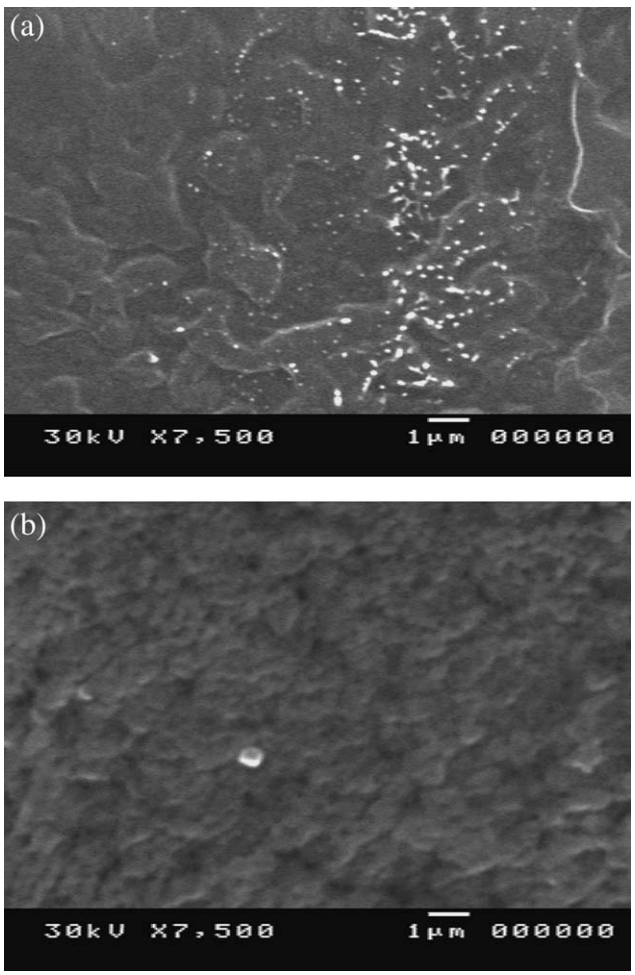

Figure 1 SEM photomicrographs of NBR–PVC/graphite for, (a) 20 phr and (b) 50 phr graphite.

are the area and the thickness of the sample, respectively), and tan δ is the dielectric loss tangent. Measurements were made at 25 K temperature intervals in the temperature range (298–423 K), maintaining a temperature rise of 1Kmin^{-1}.

Scanning electron microscopy testing

Blend samples were fractured after cooling in liquid nitrogen. The morphology of freeze fractured and microtome surfaces were characterized by using a JEOL 5410 scanning microscope (SEM). For scanning electron observation, the surface of the polymer was mounted on a standard specimen stub. A thin coating ($\sim 10^{-6}$ m) of gold was deposited onto the polymer surface and attached to the stub prior to examination in the microscope to enhance the conductivity and secondary electron emission characteristic of the overgrowth. Figure 1 shows the SEM micrographs for 20 phr [Fig. 1(a)] and 50 phr [Fig. 1(b)] graphite incorporated (30/70) NBR–PVC systems, respectively. The graphite, which appears as the inserted phase and separated by strands of polymer, is clearly noticed for 20 phr graphite loaded system. Further increase in graphite content shows the growth of second phase.

Fourier transforms infrared spectroscopy

The samples for FTIR were first prepared by using an attenuated total reflection technique. The FTIR spectra were obtained using a JASCO 460 FTIR spectrometer. The spectrum resolution was 4 cm^{-1} and the scanning range was from 1400 to 4000 cm^{-1}.

RESULTS AND DISCUSSION

Infrared spectroscopy analysis

It is well known that FTIR is a particularly suitable method to determine the presence of specific interactions between various groups in polymer blends from the force constants and it is sensitive to both inter- and intramolecular interactions.[20] In this work, we have used this technique to confirm the compatibility of the two components NBR/PVC.

Figure 2 shows the comparison of FTIR spectra of pure PVC, NBR before mixing and (50/50 PVC/NBR) after mixing blend. Pure PVC shows peak at 1641 cm^{-1}, which is due to the carbonyl groups (C=O) formed during the manufacturing stage,[21] and the polymer backbone defects,[22] and peak C—H stretching frequency just above 2900 cm^{-1}, The broad peak at 3433 cm^{-1} may be due to the formation of

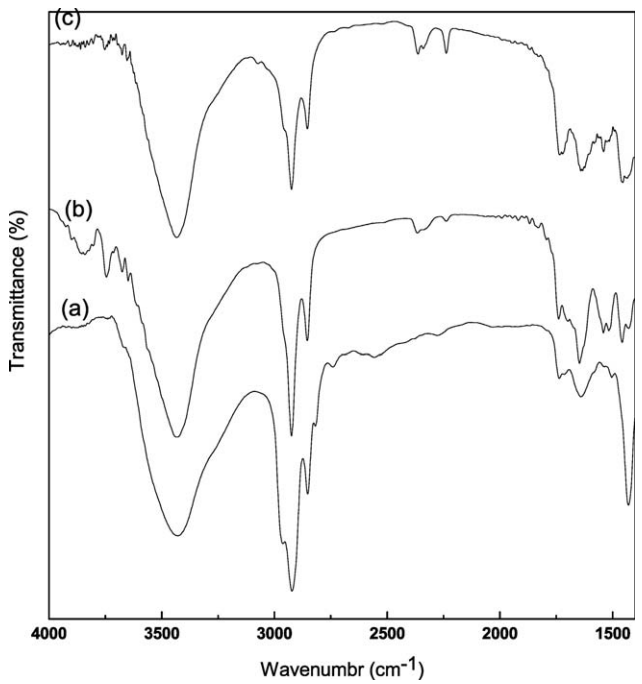

Figure 2 FTIR spectrum of PVC and NBR pre-mixing (a, PVC; b, NBR) and c, (50–50 NBR–PVC) post-mixing blends.

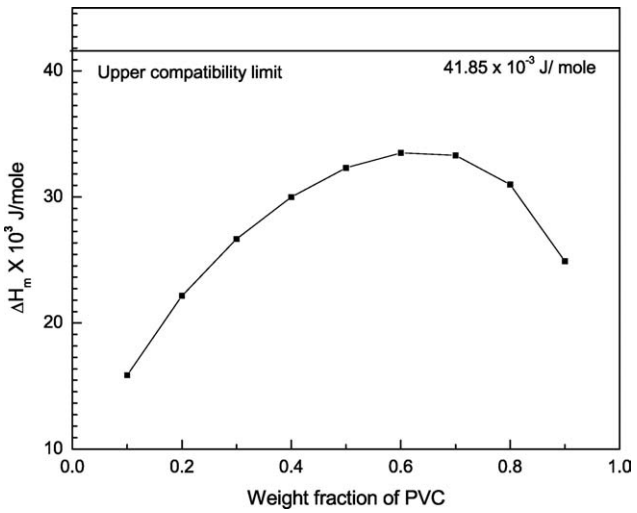

Figure 3 The relationship between the heat of mixing, and the weight fraction of PVC.

—OH groups during the degradation.[23] For pure NBR, the peak at 1646 cm^{-1} corresponds to the triazine functionality generated as a result of the cyclization of adjacent nitril groups,[24] the peak at 2237 cm^{-1} is due to the stretching vibration of the —CN group and the broad peak at 3434 cm^{-1} may be due to the formation of —OH groups during degradation. For PVC/NBR exhibits peaks at 1455 cm^{-1} corresponds to the CH_2 bending vibration, the peak center at 1734 cm^{-1} represents the carbonyl groups of ester from DOP, the olefinic C—H stretching frequency just above 2900 cm^{-1}. The peak appearing at around 2237 cm^{-1}, is attributed to the CN group from the NBR structure. The broadening and the increased absorption at 3500–3200 cm^{-1} show the formation of O-H and N-H group in the system, due to the hydrolysis of the nitrile group.[25] The results from FTIR analyses revealed strong inter-association hydrogen bonds between the nitril groups of the NBR and the carbonyl groups of PVC. This confirms the complete homogeneity of these two components with each other.

Heat of mixing method

The calculation of the heat of mixing is considered to be a tool for the determination of the degree of compatibility between polymer blends. Polymer compatibility in the solid state might occur if the heat of mixing is below 41.85×10^{-3} J/mol. The heat of Mixing, ΔH_m, was calculated for the system under investigation with the Schneier equation[26]:

$$\Delta H_m = \sqrt{X_1 M_1 \rho_1 (\delta_1 - \delta_2)^2 \left\{ X_2 / \langle (1-X_2) M_2 \rho_2 + (1-X_1) M_1 \rho_1 \rangle^2 \right\}} \quad (2)$$

where X, ρ, and M are the weight fraction of the polymer, the density, and the monomer unit molecular weight, respectively, and δ is the solubility parameter of the polymers. The obtained values are illustrated graphically in Figure 3. It is clear that the NBR–PVC blends are expected to be compatible because the calculated heat of mixing lies below the upper limit of compatibility.

Dielectric properties

The ε' and ε'' for the composite with a conductive graphite are shown in Figure 4(a,b), respectively. Both ε' and ε'' increased with increasing the graphite content at the same frequency. The larger difference of the constant values in the low frequency range was shown by the increase of graphite while at the high frequency range the difference was lowered. This means that the frequency dependence of dielectric constants was generated by the addition of

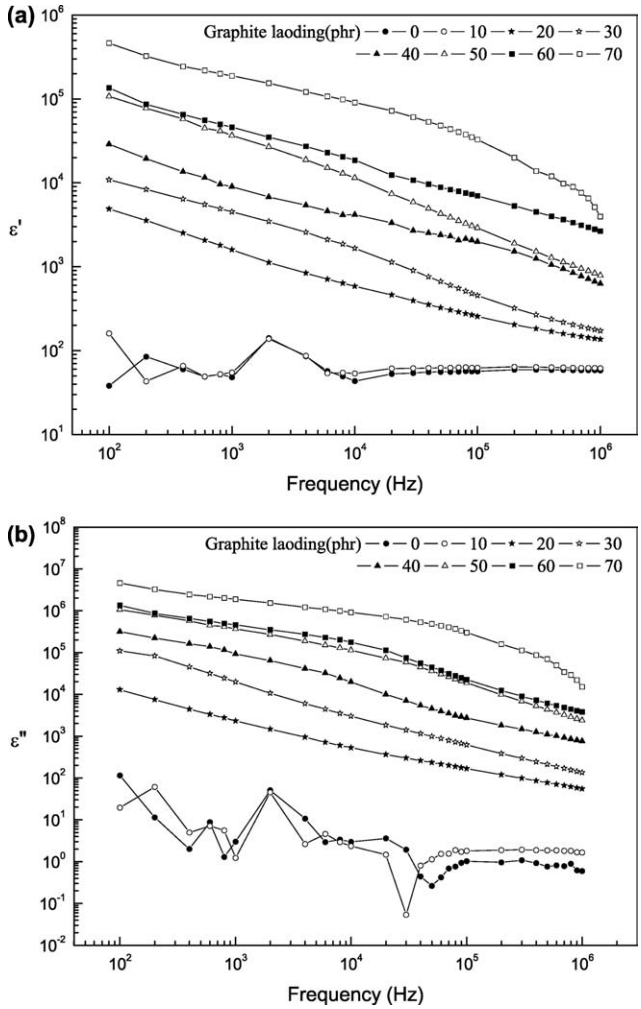

Figure 4 Complex permittivity versus frequency of PVC-NBR/graphite composites: (a) Real part of dielectric permittivity ε', and (b) dielectric losses ε''; of samples indicated on the plot.

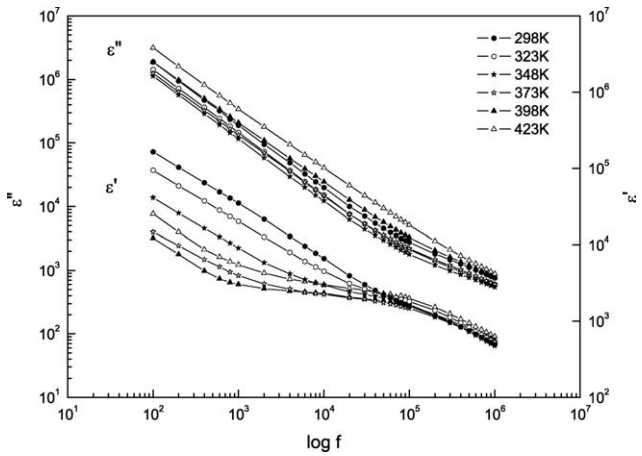

Figure 5 Logarithmic plots of complex permittivity versus frequency of PVC-NBR, with (40 phr) graphite at different temperature.

graphite. This small change of ε′ with frequency may be due to electronic interfacial polarization (the Maxwell–Wagner process) of the graphite.[27] The graphite is a semi-conductive material and does not work as dielectrics by itself. If it is covered with insulation materials, however, it shows a dielectric property by generating the space charge polarization at the interfaces. This can also be explained by Maxwell-Wagner-Sillars theory, which accounts for the dielectric loss due to the interfacial polarization of heterogeneous materials having the volume fraction of conductive filler lower than the percolation threshold.[28] The interfacial polarization can be more easily occurred at the lower frequency and/or with the number of interfaces between the graphite and matrix and, consequently, contribute to the improvement of dielectric properties of the composite filled with graphite. As the frequency is increased, the time required for the interfacial charges to be polarized or for the dipoles to be arranged is delayed,[29] and thus the frequency dependence of dielectric constant can be noticed. The sharp increase in ε″ noticed in lower frequency range is attributed to the increase in contribution of both interfacial polarization and conductivity while that for higher content of graphite is mainly due to conductivity.[30]

To study the dielectric relaxations, the frequency dependence of the total loss factor ε″ and the real part of permittivity, ε′, for G_{40}, various temperatures is represented in a log–log scale in Figure 5. All ε″ curves exhibit in the low frequency range ($f < 10^3$ Hz) a linear increase when the frequency is decreased. The experimental data are suitably fitted to the law: $\varepsilon'' = A/2\pi\varepsilon_0 f^n$ where f is the frequency of the applied electric field, the exponent n is close to 1 and the constant A is assumed to be equal to σ_{dc}[31] ε′ increases with temperature and was higher for the low frequency range. Such high values of ε′ was attributed to the interfacial effects within the bulk of the sample and the electrode effects.[32] In the high frequency range, ε′ shows a relaxation behaviour described by a sudden decrease limited by two approximately constant values of permittivity in the two sides of the relaxation frequency. For the ε″, a broad relaxation loss peak is recognized and probably associated with the relaxation of charge carriers in the bulk polymer moving via intrachain and interchain hopping.[31] When the temperature is increased, this peak shifts toward high frequencies meaning shorter relaxation time.

At low frequency range, the dc loss effect is dominant (Fig. 4) and can obscure other effects; we have then represented our data using the electric modulus defined as

$$M^* = {}^1\!/_{\varepsilon^*} = M' + iM'' \tag{3}$$

Figure 6 shows the variation of the imaginary part of the modulus as a function of frequency at increasing filler loadings. The low value of M″ in the low-frequency region suggests that electrode polarization makes negligible contribution to electric modulus at these frequencies. It can also be observed that with increase in filler loading, M″ peaks in general exhibit increasing peak heights and peak maximum shifts to higher frequencies. The M″ peaks are asymmetric and the widths are broader than ideal Debye peak thus indicating increasing Maxwell-Wagner-Sillar's polarization. The variation of M″ with increasing frequencies also shows a nonmonomodal distribution of electric modulus. At low filler loadings, the value of M″ reaches a peak value in the range of 10^3 Hz at 20 phr and around 10^4 Hz in case of 30 phr loaded samples. Further increase in filler loadings is shifting

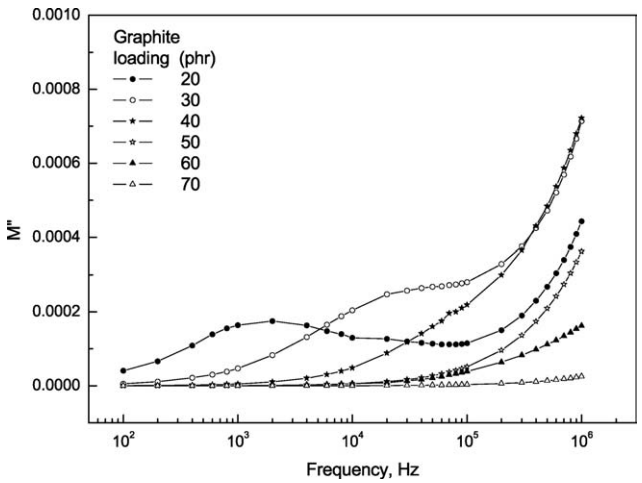

Figure 6 Variation in complex part of electric modulus with frequency at increasing graphite loadings in NBR–PVC/graphite composites.

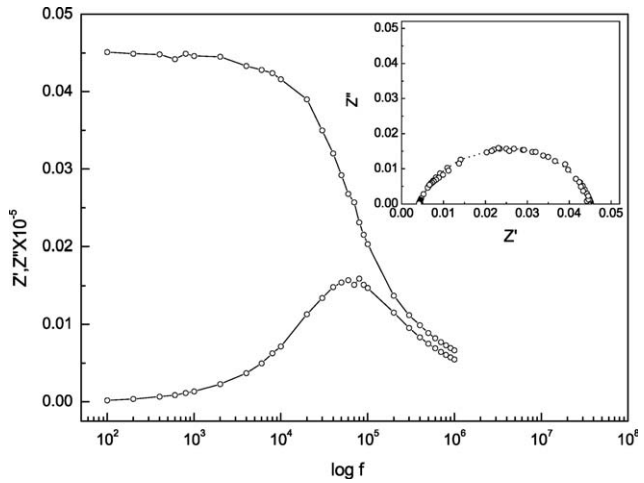

Figure 7 Frequency dependences of Z' and Z'' plot for G_{40} at 298 K together with the corresponding Cole–Cole plots in the insets.

the peak maximum to higher frequency region and could not be found due to instrumental limitations but from the trends of the graphs indicate that with increase in filler loading, the appearance of maximum value of M″ occurs at increasingly higher frequencies, which is an indication of enhanced DC conductivity as predicted by theory and given by the expression:

$$\sigma_{dc} = \frac{\varepsilon_0}{M_\infty(\tau)} \tag{4}$$

where M_∞ is the frequency at which the peak maximum occurs, (τ) is the relaxation time calculated by the expression :

$$\tau = \frac{1}{2\pi f_{\max}} \tag{5}$$

Impedance analysis

The measured impedance and phase angle were used to calculate the real (Z') and imaginary (Z'') parts of the complex impedance. Figure 7 shows the complex impedance plotted as a function of frequency for G_{40} at 298 K. From the Figure it can be observed the curve is broader than the ideal Debye curve and asymmetric. The insets show the corresponding Cole–Cole plots where an almost symmetric semicircle indicates the presence of a Debye-like relaxation. Figure 8 shows the variation of the imaginary component of the complex impedance (Z'') with frequency as a function of increasing filler loading in graphite reinforced vulcanizates. From the Figure it can be observed that with increase in frequency there is a gradual increase in complex impedance for all the vulcanizates. From the Figure, it can also be observed that with increase in filler loading there is a gradual shift of frequency, but the intensity of this shift is more pronounced at lower filler loadings than at higher filler loadings which can be attributed to the occurrence of percolation phenomenon. As graphite loading increases, the peak frequency shifts to higher values. Absolute values of the impedance get smaller with increasing graphite concentration, consistent with higher conductivity. Figure 9(a,b) shows the Cole–Cole plots of various composites as a function of filler loadings and measurement temperature. The radius of semicircle Z' indicates the electrical resistance of the composite. The Cole–Cole plot shows a semicircle for each case, which indicates a single relaxation mode and a resistive and capacitive network structure of the composite. The radius of the semicircle decreases as the amount of graphite increases and temperature decreases.

The measured impedance can be modeled by the equivalent circuit model as shown in the inset of Figure 10. To determine the nature of relaxation peak, we have analyzed the data using the impedance analog of the Havriliak–Negami function[33]:

$$\varepsilon(\omega) = \varepsilon'(\omega) - i\varepsilon''(\omega) = \varepsilon_\infty + \frac{\varepsilon_s - \varepsilon_\infty}{(1 + (i\omega\tau)^\alpha)^\beta} \tag{6}$$

where τ, α, and β are the average relaxation time, the symmetrical and asymmetrical distribution parameters for the considered relaxation peak, ε_∞ and ε_s are the dielectric constants at sufficiently higher and lower frequencies, respectively. The parameter α represents the width of the distribution while β describes the skewness of this distribution. Both parameters can take on values in the range from 0 to 1. In the case $\alpha = 0$ and $\beta = 1$ we have the well-known Debye process. The Havriliak–Negami

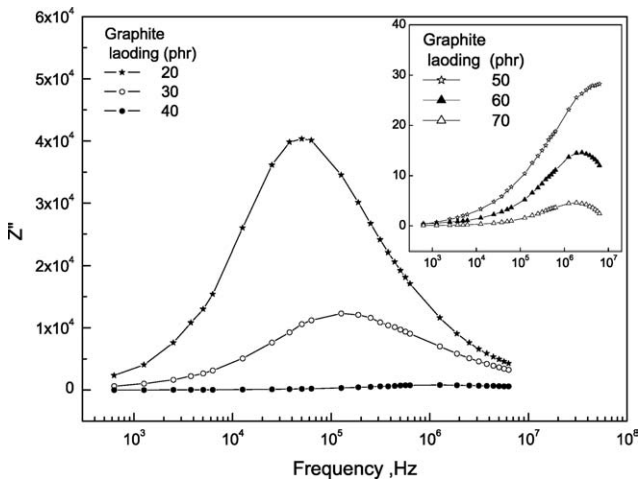

Figure 8 Variation in complex part of impedance with frequency at increasing graphite loadings in (NBR–PVC/G) composites.

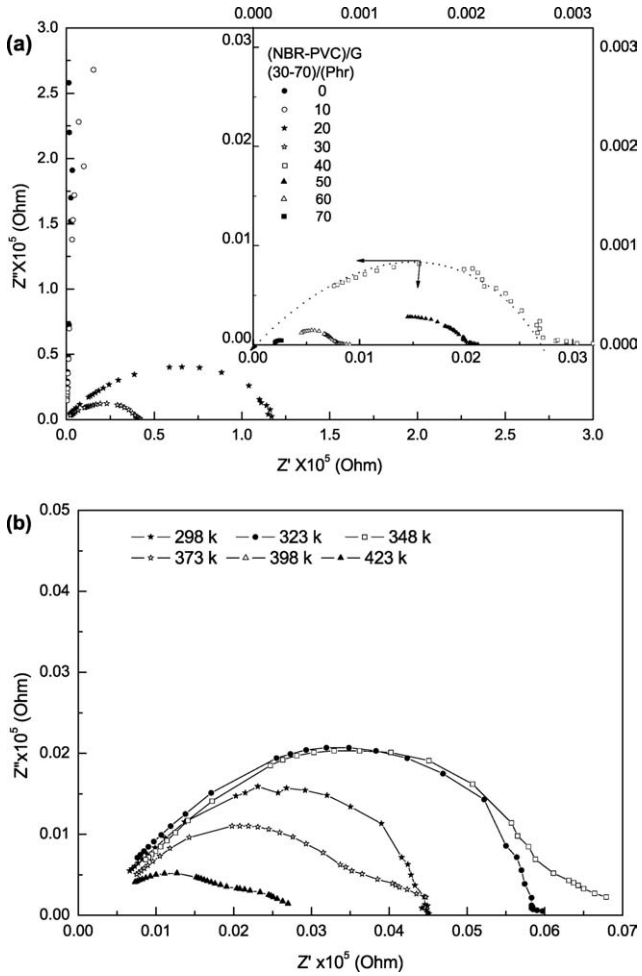

Figure 9 Complex impedance diagrams of the NBR–PVC/graphite composites as a function of graphite content and temperature: (a) at increasing graphite loadings in (NBR–PVC/graphite) composites; and (b) G_{40} at different temperature.

empirical relation can be represented by the impedance quantities since the frequency dependent data goes in the same anticlockwise direction as does for the permittivity data. Rewriting eq. (6) in the form of impedance terms:

$$Z^*(\omega) = Z_\infty + \frac{Z_s - Z_\infty}{[1 + (j\omega\tau)^\alpha]^\beta} \tag{7}$$

Separating real and imaginary terms for eq. (7):

$$Z' = Z_\infty + (Z_s - Z_\infty)A^{-1}\cos\beta\varphi \tag{8}$$

$$Z'' = (Z_s - Z_\infty)A^{-1}\sin\beta\varphi \tag{9}$$

where

$$A = \left[1 + 2(\omega\tau)^\alpha \cos\left(\frac{\alpha\pi}{2}\right) + (\omega\tau)^{2\alpha}\right]^{\beta/2} \tag{10}$$

$$\varphi = \arctan\left[\frac{(\omega\tau)^\alpha \sin(\frac{\alpha\pi}{2})}{1 + (\omega\tau)^\alpha \cos(\frac{\alpha\pi}{2})}\right] \tag{11}$$

To obtain parameters describing the relaxation mechanism in our fitting procedure we have used the complex series impedance. The fitted curves are represented in the Cole–Cole diagrams for G_{40} Figure 10. It is worth noting that at low frequencies, the fitted curves are in good agreement with the experimental data. The coincidence of the beginning of the semicircles with the origin of the graph provides a clear indication that no other relaxation process is present at lower frequencies, in the studied systems. On the other hand, the variation of the semicircles' radii is the result of the changing temperature. The parameters evaluated from the fitting procedure are listed in Table II.

AC conductivity analysis

Figure 11 shows the variation of electrical conductivity with frequency at different filler loadings. At low levels of filler loading the conductivity of the composite is slightly higher than that of the base polymer, since the filler particles are isolated from each other by the insulating polymer matrix. When the loading of filler is low, the conductivity between the grains of filler is expected to be primarily via hopping and tunneling mechanisms. In this mode of conduction, the electron transport may be coupled strongly with the molecular and ionic processes in the insulating polymer matrix. Usually, hopping transport between localized sites is the main reason for the frequency dependence of conductivity in polymer composites. The dispersion of filler is

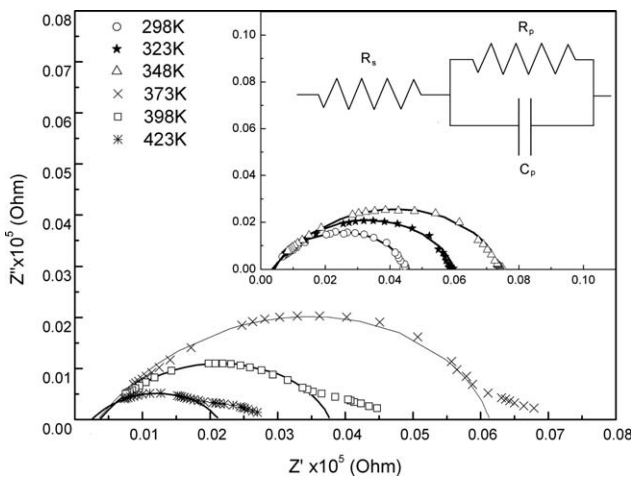

Figure 10 Cole–Cole plots of the electrical impedance of NBR–PVC with 40 (phr), graphite at different temperature: Solid curves are produced by best-fitting experimental points to the Havriliak–Negami approach (Inset: the equivalent circuit).

TABLE II
Parameters Used/Evaluated for the Havriliak-Negami Function

Graphite loading (phr)	Z_∞ (Ω)	Z_s (Ω)	α	β	T (s)
G_{20}	1,20,000	70	0.8	0.82	5.23×10^{-5}
G_{30}	41,000	60	0.78	0.71	3.28×10^{-5}
G_{40}	4520	41	0.85	0.93	2.15×10^{-6}
G_{50}	200	38	0.64	0.51	3.92×10^{-7}
G_{60}	78	32	0.74	0.93	4.16×10^{-7}
G_{70}	31	19	0.86	0.95	8.43×10^{-7}

heterogeneous, localized and disordered. This disorder results in a wide distribution of hopping rates, giving a strong dispersion of the ac conductivity.[34,35] At low frequencies, a frequency independent conductivity is recorded, which is attributed to resistive conduction through the bulk composite. On the other hand, at high frequencies, conductivity appears to be proportional to frequency due to the capacitance of the host medium between the conducting particles or clusters (conductivity is due to trapped charges which is only active at higher frequency region).[36] The frequency dependence of conductivity was increases as the additive concentration decreases (Fig. 11). It is generally thought that the observed ac conductivity takes the form[37]:

$$\sigma = \sigma_o + A\omega^s \tag{12}$$

where $\omega = 2\pi f$ is the angular frequency, A is constant and s are exponential parameter. The values of A and s calculated for increasing graphite concentrations and are shown in Table III. From the Table, it can be observed that the value of A increases and s decreases on increasing filler loading, but the intensity of this increase is less at higher loadings of filler which indicates the occurrence of percolation due to the formation of continuous filler network.

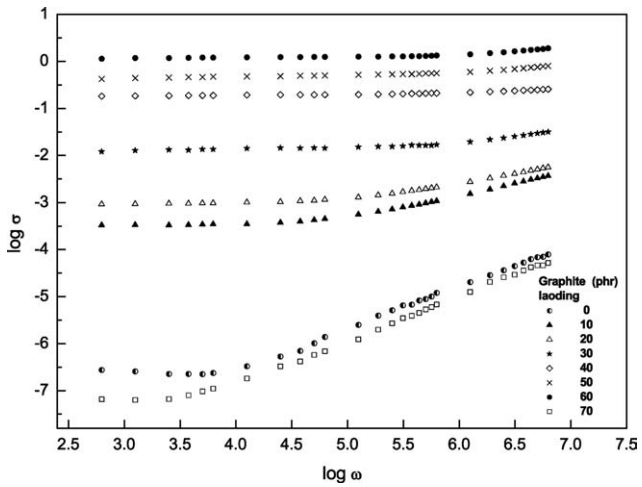

Figure 11 Frequency dependence of ac conductivity of NBR–PVC/Graphite composites for different graphite concentration at room temperature.

To better understand the influence of the temperature on the ac conductivity, the logarithmic plots of ac conductivity σ_{ac} versus temperature for PVC/NBR blend with 40 (phr), graphite is shown in Figure 12. It is evident that the ac conductivity is both frequency and temperature dependent and enhanced with increasing of both the frequency and the temperature. This indicates that there may be charge carriers, which can be transported by hopping through the defect sites along the polymer chain.[38] Several theoretical models have been proposed for the ac conduction in amorphous semiconductors such as classical hopping and quantum mechanical tunneling of charge carriers over the potential barrier separating two energetically favorable centers in a random distribution.[39,40] In electron tunneling model, s is independent of T. In case of small polaron tunneling, s increases as T increases. The variation of s with T in the examined composites systems was shown in Figure 13, It is observed that for the samples with G_0, G_{20} and G_{30}, s decreases with increasing temperature, while for the other samples, with higher graphite contents $>$ 40 phr, the curves of s exhibit a broad maxima followed by decrease of s with further increase of temperature. The small polaron hopping conduction mechanism is predominant at low temperature and

TABLE III
Comparison of Parameters Obtained From Fit the Experimental Data to $\sigma = \sigma_o + A\omega^s$ of NBR-PVC for Different Graphite Concentration at Room Temperature

Graphite loading (phr)	S	A
0	0.88	8×10^{-11}
10	0.85	1×10^{-10}
20	0.66	7×10^{-7}
30	0.55	6×10^{-6}
40	0.46	3×10^{-4}
50	0.27	2×10^{-3}
60	0.20	4×10^{-2}
70	0.11	1×10^{-1}

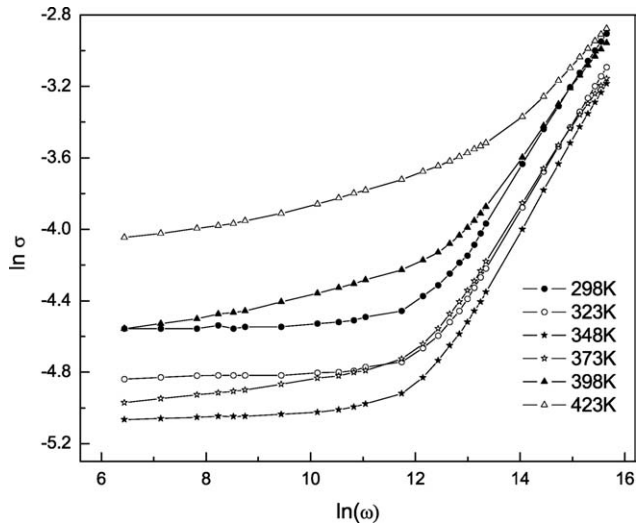

Figure 12 The ac conductivity ($\log\sigma_{ac}$) versus $\log\omega$ of the composite with 40 phr in graphite content, at various temperatures.

followed by correlated barrier hopping conduction mechanism for high temperature ($T > 350$ K). The decrease in the values of s has been interpreted by the correlated barrier hopping (C.B.H.) model.[41]

CONCLUSIONS

The dielectric studies of the acrylonitrile butadiene rubber-poly(vinyl chloride)/graphite composite clearly showed that the values of dielectric parameters, complex impedance and ac electrical conductivity are strongly depend on the frequency, temperature, and graphite loading. With increasing the filler loadings, the non semicircle nature of the Cole–Cole plots was found. This finding was based on the analysis of the resistance-capacitance circuit. The observed relaxations have been found to follow the Havriliak–Negami approach for the distribution of relaxation times. In all the investigated systems, ac conductivity exhibits a strong dispersion. At low frequencies; the conductivity tends to be constant, while at higher ones it becomes strongly frequency dependent varying approximately as a power of frequency. Interfacial or MWS relaxation in the dielectric spectra of the examined systems is due to the interfaces introduced by the graphite particles.

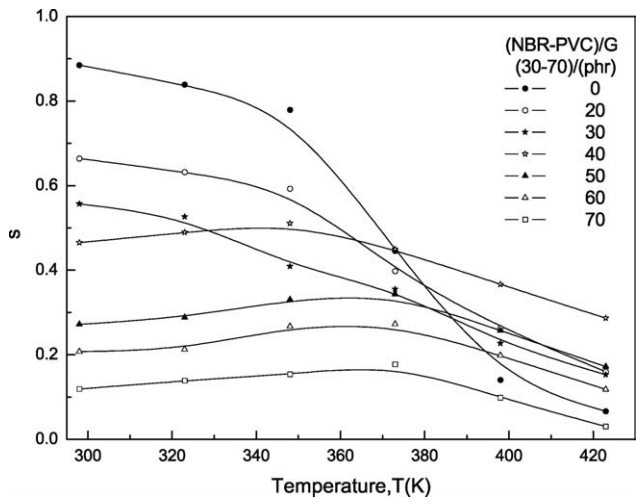

Figure 13 The variation of the parameter s with the temperature for all samples.

References

1. Celzard, A.; McRae, E.; Furdin, G.; Mareche, J. F. J Phys Condens Matter 1997, 9, 2225.
2. Celzard, A.; Mcrae, E.; Mareche, J. F.; Furdin, G.; Sundqvist B. J Appl Phys 1998; 83, 1410.
3. Zheng, Q.; Song, Y.; Wu, G.; Yi, X. J Polym Sci Part B: Polym Phys 2001; 39, 2833.
4. Krupa, I.; Novak, I.; Chodak, I. Synth Met 2004; 145, 245.
5. Lee, G. J.; Suh, K. D.; Im, S. S. Polym Eng Sci 1998; 38, 471.
6. Chodak, I.; Krupa I. J Mater Sci Lett 1999; 18, 1457.
7. Yang, G.; Tang, R.; Xiao P. Polym Compos 1997; 18, 477.
8. Nakamura, S.; Saito, K.; Sawa, G.; Kitagawa, K. Comp Jpn Appl Phys 1997; 36, 5163.
9. Stauffer, D.; Aharony, A. Introduction to Percolation Theory; Taylor & Francis: London, 1992, p 89.
10. Efros, A. L.; Shklovskii, B. I. Phys Stat Sol (b) 1976, 76, 475.
11. Li, Y. J.; Xu, M.; Feng, J. Q.; Dang Z. M. D. App Phys Lett 2006; 89, 72902.
12. Bloor, D.; Donnelly, K.; Hands, P. J.; Laughlin, P.; Lussey, D. A. J Phys D: Appl Phys 2005, 38, 2851.
13. Jiongxin, L.; Kyoung-Sik M, Jianwen, X.; Wong, C. P. J Mater Chem 2006, 16, 1543.
14. Qi, L.; Lee, B. I.; Chen, S.; Samuels, W. D.; Exarhos, G. J. Adv Mater 2005; 17, 1777.
15. Dang, Z. M.; Lin, Y. H.; Nan, C. W. Adv Mater 2003, 15, 1625.
16. Dang, Z. M.; Shen, Y.; Nan, C. W. Appl PhysLett 2002, 81, 4814.
17. Yacubowicz, J.; Narkis, M.; Benguigui, L. Polym Eng Sci 1990, 30, 459.
18. Mansour, S. A.; Al-Ghoury, M. E.; Shalaan, E.; El Eraki M. H. I.; Abdel-Bary, E. M. J Appl Poly Sci 2010, 116, 3171–3177.
19. Mansour, S. A.; Al-Ghoury, M. E.; Shalaan, E.; El Eraki M. H. I.; Abdel-Bary, E. M. J Appl Poly Sci 2010, 116, 3134–3139.
20. Huang, M.-W., Kuo, S.-W., Wu, H.-D., Chang, F.-C.; Fang, S.-Y. Polymer 2000, 41, 2479.
21. Lukas, R.; Pradora, O.; Michalcova, J.; Paleckova, V. J Polym Sci Lett 1985, 23, 85.
22. Nass, L. I., Ed. Encyclopedia of PVC; Marcel Dekker: New York, 1977.
23. Baum, D.; Wartman, L. H. J Polym Sci 1958, 28, 537.
24. Socrates, G. Infrared Characteristic Group Frequencies; Wiley Interscience, New York, 1980.
25. Manoj, N. R.; De, P. P. Polymer 1998, 39, 733.
26. Schneier, B.; J. Appl. Poly. Sci. 1973, 17, 3175.
27. Jawad, S. A.; Ahmad, M.; Ramadin, Y.; Zihlif A. Polym Int 1993, 32, 23.
28. Chung, K. T.; Sabo, A.; Pica, A. P. J Appl Phys 1982, 53, 6867.
29. Paul, A.; Thomas, S. J Appl Polym Sci 1997, 63, 247.

30. Maria, E. L.; Guilherme, M.; Ane, C.; Bluma, G.; Dipak, K. J Polym Sci Part B, Polym Phys 2003, 41, 2983.
31. Bengoechea, M. R.; Aliev F. M.; Pinto, N. J. J Phys-Condens Mat 2002, 14, 1–10.
32. Javadi, H. H. S.; Zuo, F.; Cromack, K. R.; Angelopoulos, M.; MacDiarmid, A. G.; Epstein, A. J. Synth Met 1989, 29, 409.
33. Jonscher, A. K. Universal Relaxation Law; Chelsea Dielectric Group: London, Chapter 5, 1996.
34. Ghosh, P.; Chakrabarti, A. Eur Polym J 2000, 36, 1043.
35. Bottger, H.; Bryskin, V. V. Hopping Conduction in Solids; Akademie-Verlag: Berlin, 1985.
36. de Oliveira, H. P., dos Santos, M. V. B.; dos Santos, C. G.; de Melo, C. P. Synth Met 2003, 135–136; 447–448.
37. Linden, E.; Owan, J. R. Polym J 1998, 20, 237–241.
38. Saravanan, S.; Anantharaman, M.; Venkatachalam, S. Mater Sci Eng B 2006, 135 113.
39. Rose, R. M.; Shepard, L. A.; Wulff, J. Electronic Properties; Wiley: New York, 1966; Vol. 4, p 179.
40. Dutta, P.; Biskas, S.; Ghosh, M.; De, S.; Chatterjee, S. Synth Met 2001, 122, 455.
41. Elliott, S. R. Adv Phys 1987, 2, 135.